Published by Nigerian Society of Physical Sciences. Hosted by FLAYOO Publishing House LTD

Proceedings of the Nigerian Society of Physical Sciences

Journal Homepage: https://flayoophl.com/journals/index.php/pnspsc

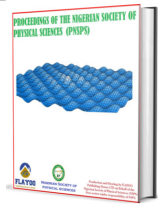

Synthesis of CuO-ZnO/banana stalk-derived activated carbon composite for efficient adsorptive removal of Cresol Red from aqueous solutions

Akeem Adebayo Jimoh[a,*], Wahaab Oluwatobi Waheed[b]

[a]*Department of Chemistry and Industrial Chemistry, PMB 1530, Kwara State University, Malete, Nigeria*
[b]*Department of Science Laboratory Technology (SLT), Federal Polytechnic Ayede, Ayede, Ogbomoso, Oyo State, Nigeria, PMB 4000*

ABSTRACT

The increasing discharge of toxic and non-biodegradable dyes from textile wastewater poses a significant environmental challenge, necessitating the development of efficient and sustainable treatment technologies. This study investigates the adsorption performance of a CuO–ZnO nanocomposite supported on banana stalk-derived activated carbon (BSAC) for the removal of Cresol Red (CR) dye from aqueous solution. The composite was synthesized via co-precipitation and characterized using X-ray diffraction (XRD), Raman spectroscopy, scanning electron microscopy (SEM), and thermogravimetric/differential thermal analysis (TGA/DTA), confirming the formation of a porous, thermally stable, and structurally integrated material. Batch adsorption experiments were conducted to evaluate the effects of pH (2–10), contact time (5–180 min), adsorbent dosage (0.01–0.10 g), and initial dye concentration. Maximum adsorption was achieved at an equilibrium concentration of 100 mg L^{-1}, pH 6, 0.01 g dosage, and 30 min contact time, with an adsorption capacity of 178.8 mg g^{-1}. Kinetic analysis revealed that the adsorption followed the pseudo-second-order model (R^2 = 0.9932), indicating chemisorption as the dominant mechanism. Equilibrium data were best described by the Temkin isotherm, while the Freundlich model further suggested multilayer adsorption on a heterogeneous surface. The results demonstrate that the CuO–ZnO/BSAC composite is a low-cost, sustainable, and efficient adsorbent with strong potential for application in dye-contaminated wastewater treatment.

Keywords: CuO–ZnO nanocomposite, Activated carbon, Cresol red dye, Adsorption, Wastewater treatment.

DOI:10.61298/pnspsc.2026.3.345

1. INTRODUCTION

The rapid growth of the textile industry has significantly contributed to global economic development; however, it has also emerged as one of the most critical sources of environmental pollution because of the large-scale discharge of untreated dye-laden wastewater [1]. Textile effluents are complex and highly contaminated, containing a wide range of synthetic dyes, auxiliary chemicals, and heavy metals that resist natural degradation processes. The persistence and recalcitrant nature of these pollutants have raised serious environmental concerns, particularly in developing and industrialized regions where wastewater treatment infrastructure is often inadequate [2].

It is estimated that more than 70 million tonnes of synthetic

*Corresponding Author Tel. No.: +234-803-2422-513.
e-mail: akeem.jimoh@kwasu.edu.ng (Akeem Adebayo Jimoh)

dyes are produced annually worldwide, with a considerable fraction released into aquatic environments during textile processing because of inefficient dye-fixation mechanisms [3]. These dyes, including azo, reactive, acid, and disperse dyes, possess complex aromatic molecular structures that confer high stability against light, heat, and microbial attack. Consequently, they persist in water bodies for extended periods, leading to severe ecological and health-related consequences [4]. The discharge of dye-containing effluents reduces light penetration, disrupts photosynthetic activity in aquatic systems, and contributes to increased biochemical oxygen demand (BOD) and chemical oxygen demand (COD), ultimately resulting in oxygen depletion and ecosystem imbalance [5].

In addition to dyes, textile wastewater often contains toxic heavy metals such as chromium, cadmium, mercury, lead, and arsenic, as well as various organic additives used during processing operations such as sizing, bleaching, and finishing. These contaminants can bioaccumulate in living organisms and biomagnify through the food chain, posing long-term risks including mutagenicity, carcinogenicity, and organ toxicity [6, 7]. The complex composition and high variability of textile effluents make their treatment particularly challenging, necessitating the development of efficient and sustainable remediation strategies.

Conventional wastewater treatment methods, including coagulation–flocculation, advanced oxidation processes, membrane filtration, and biological treatments, have been widely applied for dye removal. However, these techniques often have important limitations, such as high operating costs, energy requirements, incomplete removal of recalcitrant compounds, and generation of secondary pollutants [6, 8]. As a result, adsorption has gained considerable attention as a promising alternative because of its operational simplicity, high efficiency, and economic feasibility.

In recent years, adsorption research has shifted toward the development of low-cost, eco-friendly, and high-performance adsorbents derived from renewable resources. Agricultural wastes, particularly lignocellulosic biomass, have emerged as attractive precursors for activated carbon production because of their abundance, low cost, and favorable physicochemical properties. Among these materials, banana stalk is a readily available and underutilized biomass with high carbon content and inherent porosity, making it a suitable candidate for sustainable adsorbent synthesis [9, 10].

To further enhance adsorption performance, surface modification and composite formation with metal oxides have been extensively explored. Metal oxides such as copper oxide (CuO) and zinc oxide (ZnO) exhibit unique physicochemical properties, including high surface reactivity, photocatalytic activity, and strong affinity for organic pollutants. The integration of these metal oxides with biomass-derived activated carbon can create synergistic effects, resulting in improved adsorption capacity, enhanced surface functionality, and increased availability of active sites [11, 12]. Despite these advantages, studies on CuO–ZnO-supported biomass-derived activated carbon composites, particularly from banana stalk, remain relatively limited, highlighting a significant research gap.

Furthermore, understanding the adsorption mechanism is crucial for optimizing adsorbent performance and scaling up for practical applications. This requires comprehensive evaluation using adsorption isotherm and kinetic models to elucidate the interaction between adsorbate and adsorbent, as well as the rate-controlling steps governing the process [13, 14].

Therefore, the present study aims to synthesize a novel CuO–ZnO nanocomposite supported on banana stalk-derived activated carbon and evaluate its efficiency for removing Cresol Red dye from aqueous solutions. The study also investigates adsorption behavior through equilibrium isotherm and kinetic modeling, thereby providing valuable insight into the adsorption mechanism and the potential application of the developed material in sustainable wastewater treatment.

2. MATERIALS AND METHODS

2.1. MATERIALS

All reagents used were of analytical grade and were purchased from Sigma-Aldrich (USA) and BDH (UK). Cresol Red dye, hydrochloric acid (HCl), and sodium hydroxide (NaOH) were used without further purification. Banana stalks were collected locally, washed, and dried.

2.2. PREPARATION OF ACTIVATED CARBON

The dried banana stalks were carbonized at 500 °C for 2 h under limited oxygen conditions. The resulting carbon was activated using 2 M HNO_3 for 24 h and was washed to neutral pH and dried at 110 °C to obtain banana stalk activated carbon (BSAC) [15].

2.3. SYNTHESIS OF CUO–ZNO COMPOSITE

The CuO–ZnO nanocomposite was synthesized via a co-precipitation technique using zinc nitrate and copper nitrate at a 2:1 molar ratio, with a slight modification of the method reported in Ref. [16]. The mixture was precipitated at pH 10, aged, filtered, dried, and calcined at 400–500 °C to obtain the final composite.

2.4. CHARACTERIZATION OF THE CUO–ZNO COMPOSITE

The synthesized CuO–ZnO composite was characterized to determine its structural, morphological, and thermal properties. X-ray diffraction (XRD) analysis was performed to identify the crystalline phases present in the material. Raman spectroscopy was used to investigate the molecular structure and bonding characteristics of the composite. Surface morphology and particle distribution were examined using scanning electron microscopy (SEM). Thermogravimetric and differential thermal analyses (TGA/DTA) were conducted to evaluate the thermal stability and decomposition behavior of the material. These characterization techniques provided comprehensive information on the physicochemical properties of the synthesized adsorbent.

2.5. ADSORPTION EXPERIMENTS

Batch adsorption experiments were conducted in 250 mL Erlenmeyer flasks by contacting 0.01–0.10 g of CZ–BSAC composite with 30 mL of Cresol Red solution at an initial concentration of 100 mg L^{-1}. The effect of contact time was investigated over 5–180 min (5, 10, 20, 30, 60, 120, and 180 min), while the solution pH was adjusted between 2 and 10 using 2 M HCl and 2 M

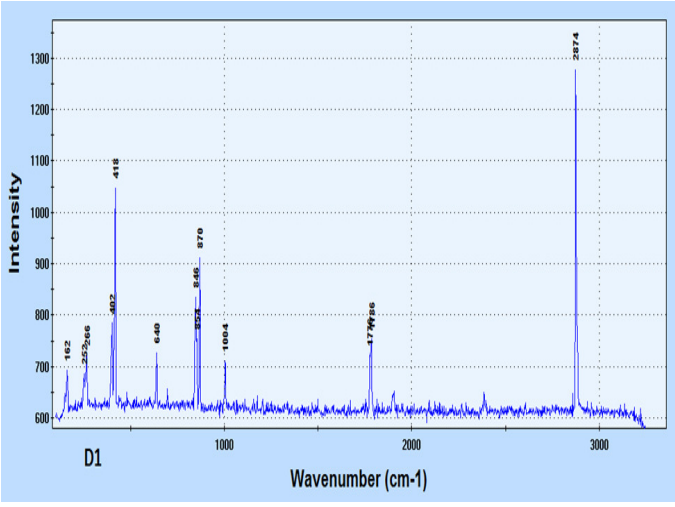

(a) Raman spectrum.

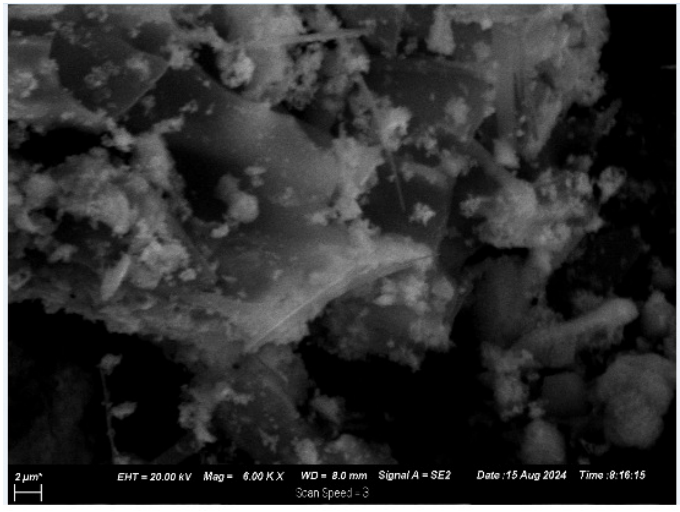

(b) SEM micrograph.

Figure 1. Characterization of the CuO–ZnO composite: (a) Raman spectrum and (b) SEM micrograph.

Table 1. Summary of isotherm study on the adsorption of Cresol Red dye onto the CuO–ZnO composite.

Isotherm model	Parameter	Value	Unit
Freundlich	R^2	0.7194	—
	K_f	0.5678	$(\text{mg g}^{-1})(\text{L mg}^{-1})^{1/n}$
	n	2.2016	—
Langmuir	R^2	0.4883	—
	$q_{\max}$	67.02	mg g^{-1}
	K_L	0.3325	L mg^{-1}
	R_L	0.015–0.231	—
Temkin	R^2	0.9754	—
	A	5.0968	L g^{-1}
	B	0.0133	J mol^{-1}

Table 2. Summary of kinetic study on the adsorption of Cresol Red dye onto the CuO–ZnO composite.

Kinetic model	R^2	Rate constant	Calculated parameter	Unit
Pseudo-first-order	0.6072	$k_1 = 0.00712$	q_e (cal.) = 39.001	min^{-1}
Pseudo-second-order	0.9932	$k_2 = 7.17 \times 10^{-7}$	q_e (cal.) = 178.810; q_e (exp.) = 183.512	$\text{g mg}^{-1}\ \text{min}^{-1}$
Intraparticle diffusion	0.5102	$k_{id} = 0.0602$	$C = -1.514$	mg g^{-1}

NaOH where applicable. The influence of adsorbent dosage was evaluated using 0.01, 0.02, 0.04, 0.06, and 0.10 g per flask.

At the end of each adsorption period, the suspensions were separated by vacuum filtration using Whatman No. 42 filter paper. The residual concentration of Cresol Red (C_e) in the filtrate was determined by measuring absorbance at 433 nm using a UV–Vis spectrophotometer (Model AVI-721). All experiments were performed in triplicate, and the results are presented as mean values ± standard deviation.

The percentage of Cresol Red adsorbed and the quantity adsorbed were calculated using Eqs. (1) and (2), respectively:

$$\text{Percentage adsorbed (\%)} = \frac{C_0 - C_e}{C_0} \times 100, \tag{1}$$

$$q_e = \frac{(C_0 - C_e)V}{m}, \tag{2}$$

where C_0 and C_e are the Cresol Red concentrations (mg L^{-1}) before and after adsorption, respectively; V is the Cresol Red solution volume; and m is the adsorbent mass.

2.6. ADSORPTION MODELING

2.6.1. Isotherm model study

Adsorption equilibrium data were analyzed using the Langmuir, Freundlich, and Temkin isotherm models to describe the interaction between Cresol Red molecules and the CZ–BSAC composite surface.

The Langmuir isotherm assumes monolayer adsorption on a homogeneous surface with a finite number of identical sites and

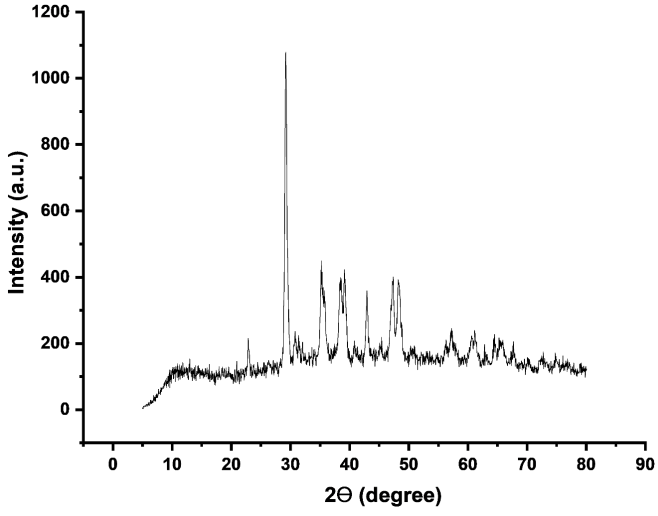

(a) X-ray diffractogram.

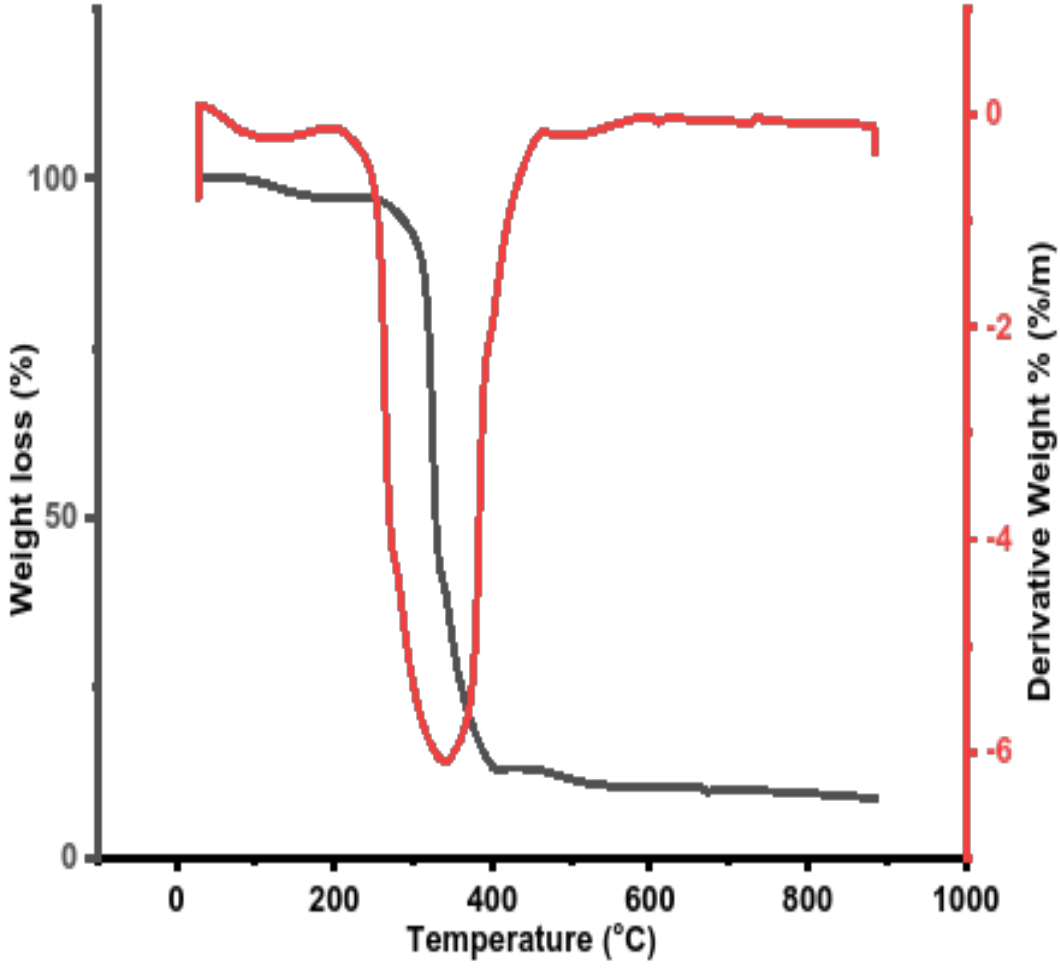

(b) TGA/DTA curve.

Figure 2. Characterization of the CuO–ZnO composite: (a) X-ray diffractogram and (b) TGA/DTA graph.

is expressed as

$$\frac{C_e}{q_e} = \frac{1}{q_o K_L} + \frac{1}{q_o} C_e, \tag{3}$$

$$R_L = \frac{1}{1 + K_L C_o}, \tag{4}$$

where C_e is the equilibrium concentration (mg L^{-1}), q_e is the quantity adsorbed at equilibrium (mg g^{-1}), q_o is the optimal monolayer coverage of the quantity adsorbed on the adsorbent surface (mg g^{-1}), and K_L is the Langmuir constant (L mg^{-1}).

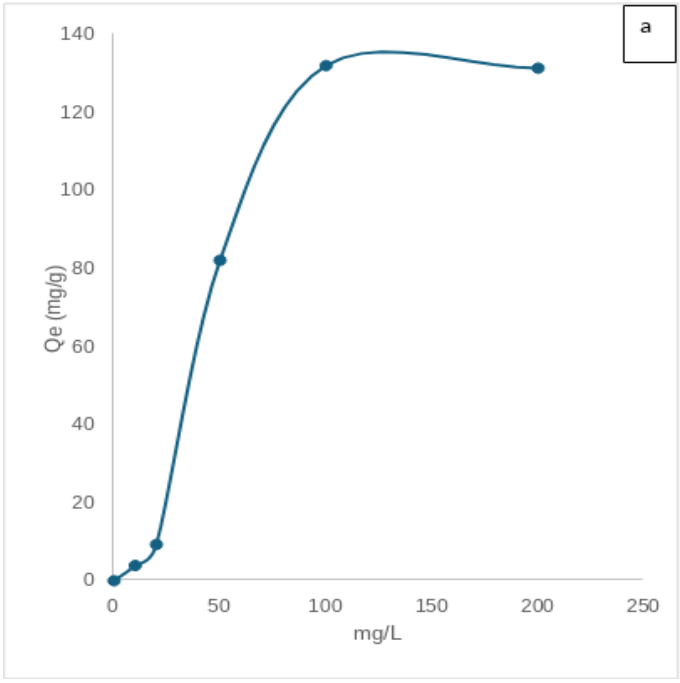

(a) Initial concentration.

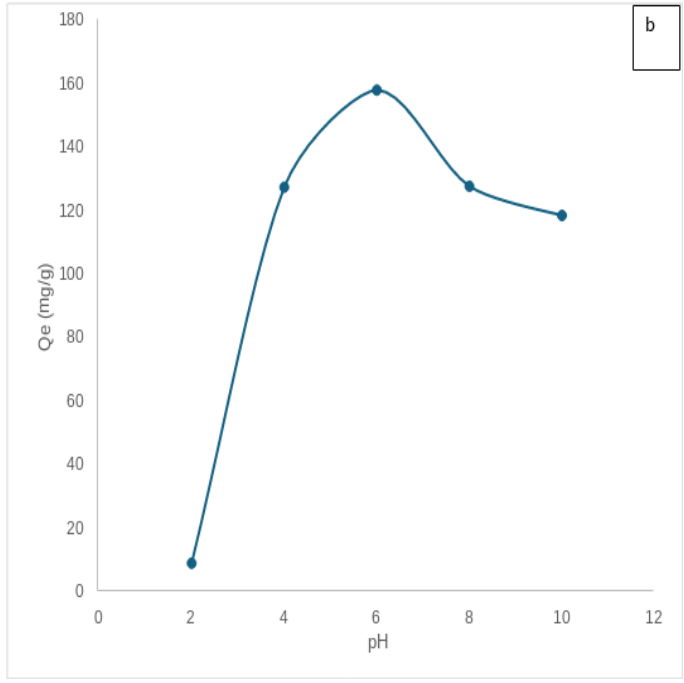

(b) Solution pH.

Figure 3. Effects of (a) initial Cresol Red dye concentration and (b) solution pH on the adsorption of Cresol Red dye onto the CuO–ZnO composite.

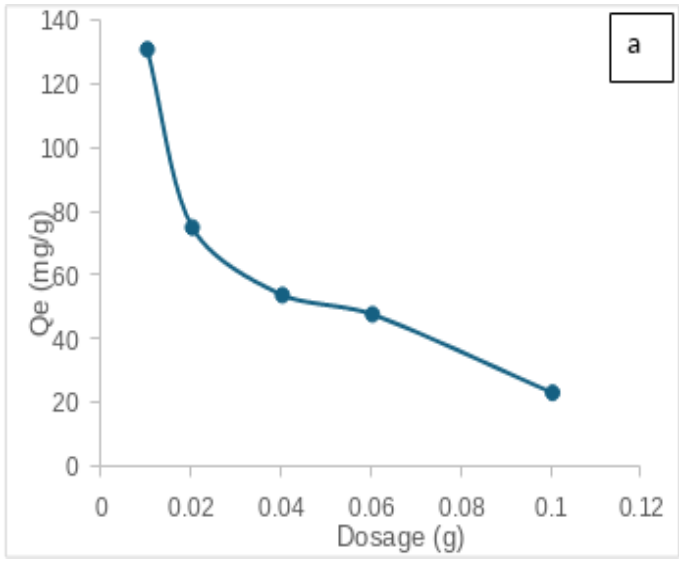

(a) Adsorbent dosage.

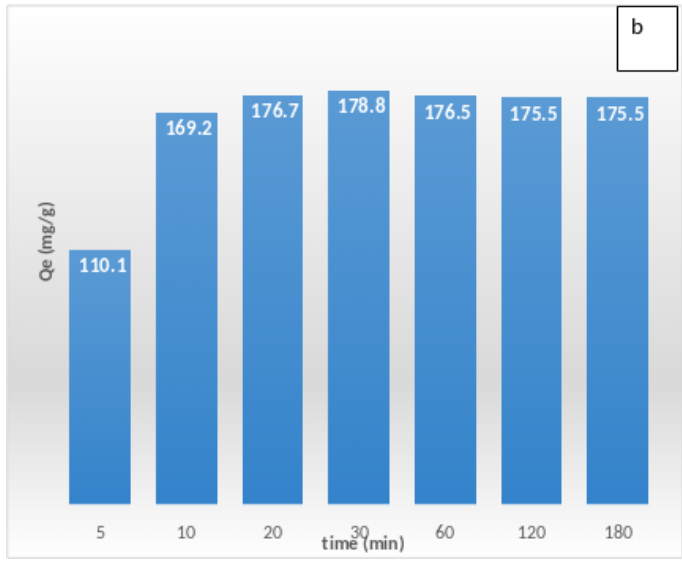

(b) Contact time.

Figure 4. Effects of (a) adsorbent dosage and (b) contact time on the adsorption of Cresol Red dye onto the CuO–ZnO composite.

The Freundlich isotherm is represented as

$$\log q_e = \frac{1}{n} \log C_e + \log K_f, \tag{5}$$

where K_f is the Freundlich adsorption exponent and $1/n$ is the Freundlich distribution coefficient of the average adsorption capacity of the solid.

The Temkin isotherm considers adsorbent–adsorbate interactions and assumes that the heat of adsorption decreases linearly with surface coverage:

$$q_e = \frac{RT}{b_T} \ln A_T + \frac{RT}{b_T} \ln C_e, \tag{6}$$

where A_T is the equilibrium binding constant (L g^{-1}), b_T is the Temkin isotherm constant, R is the universal gas constant (8.314 J mol^{-1} K^{-1}), and T is the temperature (298 K).

2.6.2. Kinetic model study

The adsorption kinetics were evaluated using pseudo-first-order, pseudo-second-order, and intraparticle diffusion models to deter-

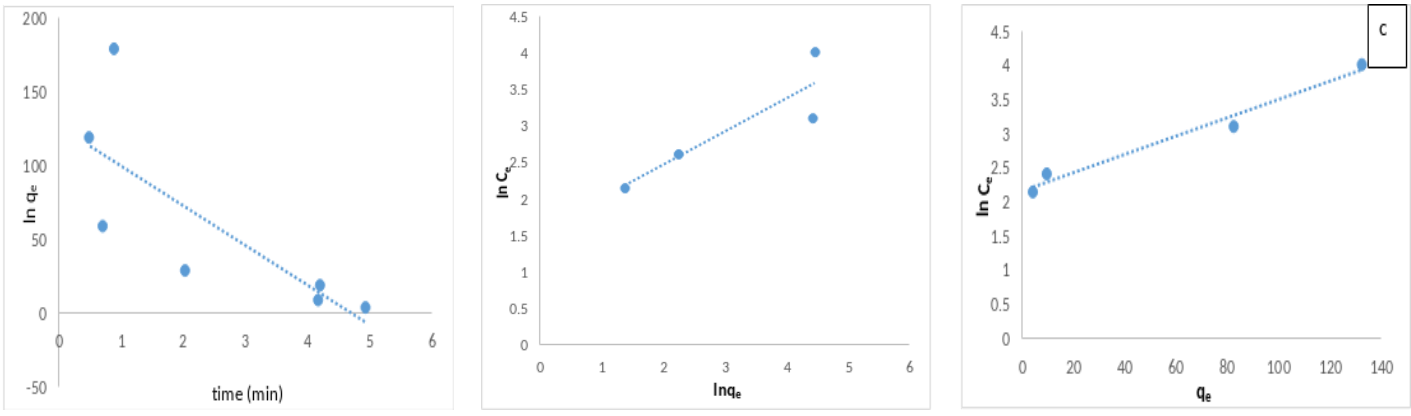

(a) Langmuir. (b) Freundlich. (c) Temkin.

Figure 5. Isotherm study plots for the adsorption of Cresol Red dye onto the CuO–ZnO composite: (a) Langmuir, (b) Freundlich, and (c) Temkin.

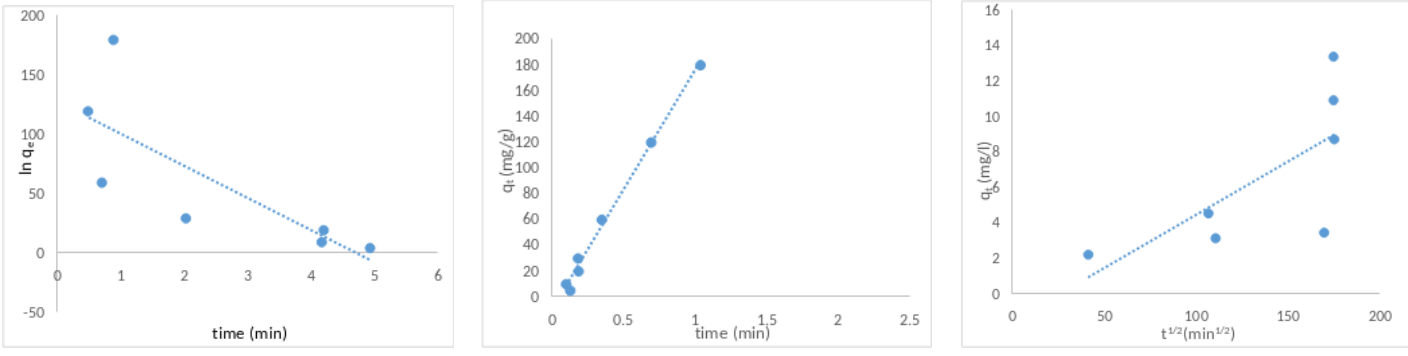

(a) Pseudo-first-order. (b) Pseudo-second-order. (c) Intraparticle diffusion.

Figure 6. Kinetic study plots for the adsorption of Cresol Red dye onto the CuO–ZnO composite: (a) pseudo-first-order, (b) pseudo-second-order, and (c) intraparticle diffusion.

mine the adsorption rate and mechanism.

The pseudo-first-order model is expressed as

$$\ln(q_e - q_t) = \ln q_e - k_1 t, \tag{7}$$

where q_t is the quantity adsorbed at time t (mg g^{-1}), t is the contact time of adsorption (min), and k_1 is the adsorption constant for the pseudo-first-order model.

The pseudo-second-order kinetic model is given as

$$\frac{t}{q_t} = \frac{1}{k_2 q_e^2} + \frac{t}{q_e}, \tag{8}$$

where k_2 is the adsorption constant for the pseudo-second-order model.

The intraparticle diffusion equation is expressed as

$$q_t = k_{id} t^{1/2} + C_{id}, \tag{9}$$

where k_{id} is the adsorption constant for the intraparticle diffusion model and C_{id} is the boundary-layer constant.

3. RESULTS AND DISCUSSION

3.1. CHARACTERIZATION OF THE CUO–ZNO COMPOSITE

As shown in Figure 1(a), the Raman spectrum of the CuO–ZnO composite confirms the successful formation of the metal oxide system. The characteristic vibrational bands observed in the spectrum correspond to the intrinsic phonon modes of CuO and ZnO phases, consistent with Ref. [17]. The presence of distinct peaks associated with Cu–O and Zn–O lattice vibrations indicates that both oxides are successfully incorporated within the composite structure without significant phase distortion. The absence of additional impurity bands suggests high phase purity and effective synthesis of the CuO–ZnO composite. Furthermore, the slight peak broadening may be attributed to reduced crystallite size and increased lattice strain resulting from strong interfacial interactions between CuO and ZnO particles [12].

Figure 1(b) presents the SEM micrograph analysis of the CuO–ZnO composite. The SEM image reveals an irregular and heterogeneous surface morphology with agglomerated nanoparticles distributed across the surface. This rough and porous texture is beneficial for adsorption applications because it provides more active sites for dye molecule interaction. The uniform distribution of these elements suggests successful integration of CuO and ZnO phases within the composite matrix, which is essential for synergistic adsorption performance [18].

The X-ray diffractogram presented in Figure 2(a) further validates the crystalline nature of the CuO–ZnO composite. The diffraction peaks correspond well to the monoclinic and hexagonal phases of CuO (JCPDS-48-1548) and ZnO (JCPDS-36-1451), respectively [19], indicating successful formation of a heterostructured composite without formation of undesired sec-

ondary phases. The sharp and well-defined peaks confirm the crystalline nature of the material, while slight peak broadening suggests nanocrystalline behavior. The characteristic peaks at 31.7°, 34.4°, and 36.2° (2θ) correspond to the (100), (002), and (101) planes of hexagonal ZnO, while the peak at 38.7° (2θ) is assigned to the (111) plane of monoclinic CuO [20]. Slight broadening of the diffraction peaks indicates nanocrystalline properties, while the sharp diffraction peaks confirm the crystalline nature of the composite. Furthermore, an amorphous carbon peak can be seen around 26° (2θ), which is attributed to the amorphous carbon of the biomass precursor. The coexistence of both CuO and ZnO diffraction peaks supports the formation of a composite rather than a single-phase material, which is advantageous for enhancing adsorption through synergistic surface interactions and increased active-site availability [12].

Figure 2(b) illustrates the thermogravimetric analysis (TGA) and differential thermal analysis (DTA) curves of the CuO–ZnO composite. The TGA curve indicates high thermal stability of the composite, with minimal weight loss observed over a broad temperature range. The initial small weight loss usually observed at lower temperatures (150–200 °C) is assumed to be due to evaporation of physically adsorbed water molecules and desorption of volatile surface impurities that are not strongly bound to the surface of the adsorbent [21]. The absence of significant decomposition at higher temperatures confirms the strong thermal stability of the metal oxide framework. The corresponding DTA curve shows weak thermal events, further supporting the stability of the composite structure. This thermal robustness makes the CuO–ZnO composite suitable for practical wastewater treatment applications under varying environmental conditions.

The combined characterization results confirm the successful synthesis of a structurally stable CuO–ZnO composite with well-defined morphology, high crystallinity, and excellent thermal stability, all of which are essential properties for efficient adsorption of dye pollutants.

3.2. BATCH ADSORPTION STUDIES

As shown in Figure 3(a), the effect of initial Cresol Red concentration on adsorption performance indicates that the adsorption capacity of the CuO–ZnO composite increases with increasing dye concentration, reaching a maximum adsorption value of 132.15 mg g^{-1} at 100 mg L^{-1}. This trend is attributed to the increased driving force for mass transfer at higher dye concentrations, which enhances the diffusion of dye molecules from the bulk solution to the adsorbent surface. At lower concentrations, fewer dye molecules are available to occupy active sites, resulting in lower adsorption capacity. However, at higher concentrations, although adsorption capacity increases, percentage removal efficiency may decrease because of saturation of available adsorption sites [22].

Figure 3(b) illustrates the influence of solution pH on the adsorption process. The adsorption capacity increased with increasing pH and reached a maximum at pH 6, which was identified as the optimum condition for the removal of 158.1 mg g^{-1} of Cresol Red. At low pH values, the adsorbent surface is highly protonated, leading to electrostatic repulsion between the dye molecules and the surface, thereby reducing adsorption. As the pH increases toward neutral conditions, electrostatic attraction and other interactions, such as hydrogen bonding, become more favorable, enhancing adsorption. Beyond pH 6, a decrease in adsorption capacity was observed, likely because of competition from hydroxyl ions (OH^-) and possible structural changes in the dye molecules [23].

The effect of adsorbent dosage is presented in Figure 4(a), where the adsorption capacity was highest at the lowest dosage of 0.01 g. At this dosage, the available active sites are fully accessible, leading to efficient utilization of the adsorbent surface. As adsorbent dosage increases, the adsorption capacity per unit mass decreases because of particle aggregation and overlapping of active sites, which reduce the effective surface area. Additionally, at higher dosages, the ratio of dye molecules to available active sites decreases, leading to underutilization of the adsorbent [24].

Figure 4(b) shows the effect of contact time on the adsorption of Cresol Red. The adsorption capacity increased rapidly during the initial stage and reached a maximum at approximately 30 min, with an adsorption capacity of 178.8 mg g^{-1}, indicating the optimum contact time for the adsorption process. This rapid uptake is attributed to the abundance of vacant active sites at the initial stage. After 30 min, the adsorption rate decreased and approached equilibrium, suggesting that most active sites had been occupied and that further adsorption was limited by slower diffusion processes within the pores of the adsorbent [25, 26].

3.3. ISOTHERM ANALYSIS OF CRESOL RED DYE ADSORPTION ONTO THE CZ–BSAC COMPOSITE

As presented in Table 1, the adsorption behavior of Cresol Red onto the CZ–BSAC composite was evaluated using Langmuir, Freundlich, and Temkin isotherm models to better understand the adsorption mechanism and surface characteristics of the adsorbent.

The Langmuir isotherm model, which assumes monolayer adsorption on a homogeneous surface with identical binding sites, showed a poor fit to the experimental data, as indicated by the low regression coefficient (R^2 = 0.4883). This suggests that the adsorption process does not conform to the ideal Langmuir assumptions. The maximum monolayer adsorption capacity (q_{max} = 67.02 mg g^{-1}) is relatively low, further indicating that monolayer coverage is not the dominant mechanism. However, the Langmuir constant (K_L = 0.3325 L mg^{-1}), which reflects the affinity between adsorbate and adsorbent, indicates moderate interaction strength. The dimensionless separation factor (R_L), calculated in the range 0.015–0.231, falls between 0 and 1, confirming that the adsorption of Cresol Red onto CZ–BSAC is thermodynamically favorable despite the poor overall model fit [27].

In contrast, the Freundlich isotherm model provided a better representation of the adsorption process, with a higher regression coefficient (R^2 = 0.7194). The Freundlich constant (K_f = 0.5678) suggests moderate adsorption capacity, while the adsorption intensity factor (n = 2.2016) lies within the favorable range ($1 < n < 10$), indicating that adsorption is spontaneous and favorable [28]. The applicability of the Freundlich model suggests that adsorption occurs on a heterogeneous surface with a non-uniform distribution of active sites and that multilayer adsorption is likely. This behavior is consistent with the porous and irregular morphology observed in the SEM analysis [29].

The Temkin isotherm model exhibited the best fit among all

models, with a high regression coefficient (R^2 = 0.9754), indicating that it most accurately describes the adsorption process. The Temkin constant (A = 5.0968 L g^{-1}) reflects a relatively strong binding interaction between Cresol Red molecules and the CZ–BSAC composite [30]. The Temkin heat of adsorption constant (B = 0.0133 J mol^{-1}) suggests that the heat of adsorption decreases linearly with increasing surface coverage, which is characteristic of adsorbent–adsorbate interactions involving heterogeneous surfaces. The good agreement with the Temkin model implies that adsorption is influenced by indirect interactions between adsorbed molecules and that energy distribution across the surface is not uniform [30].

The isotherm analysis reveals that the adsorption of Cresol Red onto CZ–BSAC is best described by the Temkin model, followed by the Freundlich model, while the Langmuir model shows poor applicability. This indicates that the adsorption mechanism is governed by heterogeneous surface interactions, multilayer adsorption, and a progressive decrease in adsorption energy with increasing surface coverage. These findings further support the roles of both the metal oxide components and the activated carbon matrix in providing diverse active sites and enhancing adsorption performance [31].

3.4. KINETIC STUDY OF CRESOL RED DYE ADSORPTION ONTO THE CUO–ZNO COMPOSITE

The kinetic analysis (Table 2) of Cresol Red adsorption onto the CZ–BSAC composite was carried out using pseudo-first-order, pseudo-second-order, and intraparticle diffusion models to clarify the adsorption mechanism and rate-controlling steps. The pseudo-first-order model showed poor agreement with the experimental data (R^2 = 0.6072), with k_1 = 0.00712 min^{-1} and calculated q_e = 39.001 mg g^{-1}, which deviates significantly from the experimental value (183.512 mg g^{-1}), indicating that physisorption and liquid-film diffusion are not dominant mechanisms [14]. In contrast, the pseudo-second-order model provided an excellent fit (R^2 = 0.9932), with $k_2 = 7.17 \times 10^{-7}$ g mg^{-1} min^{-1} and calculated q_e = 178.810 mg g^{-1}, closely matching the experimental q_e (183.512 mg g^{-1}; 1.3% error), confirming chemisorption as the primary rate-controlling mechanism involving valence interactions and electron sharing between Cresol Red and CuO–ZnO active sites on the CZ–BSAC surface [14].

The intraparticle diffusion model exhibited low correlation (R^2 = 0.5102), with k_{id} = 0.0602 mg g^{-1} min$^{-1/2}$ and a negative intercept (C = −1.514), indicating that intraparticle diffusion is not the sole rate-limiting step, while the non-zero intercept suggests boundary-layer effects with a minor pore-diffusion contribution [32]. The adsorption kinetics are best described by the pseudo-second-order model, confirming chemisorption dominance with secondary film-diffusion influence and negligible intraparticle diffusion in the CZ–BSAC/Cresol Red system.

4. CONCLUSION

This study successfully demonstrated the synthesis and application of a visible-light-responsive CuO–ZnO nanocomposite supported on banana stalk-derived activated carbon (BSAC) for the efficient removal of Cresol Red from aqueous solution. Characterization results confirmed the formation of a crystalline, thermally stable, and porous heterostructured composite with well-distributed CuO and ZnO phases anchored on the activated carbon matrix, providing abundant active sites for adsorption. Batch adsorption studies revealed that removal efficiency was strongly influenced by solution pH, contact time, adsorbent dosage, and initial dye concentration, with optimal performance achieved at pH 6, 100 mg L^{-1} dye concentration, 0.01 g adsorbent dosage, and 30 min contact time, yielding a maximum adsorption capacity of 178.8 mg g^{-1}.

Equilibrium and kinetic modeling indicated that the adsorption process is best described by the Temkin isotherm, suggesting heterogeneous surface interactions and energy-dependent adsorption behavior, while the Freundlich model further confirmed multilayer adsorption. Kinetic analysis revealed that the process follows a pseudo-second-order model, confirming chemisorption as the dominant rate-controlling mechanism, with limited contribution from intraparticle diffusion and secondary boundary-layer effects.

The CuO–ZnO/BSAC composite exhibits high adsorption efficiency, rapid uptake, and strong surface reactivity, making it a promising, low-cost, and sustainable adsorbent for the treatment of dye-contaminated wastewater. The integration of agricultural waste-derived activated carbon with metal oxide nanostructures provides a viable pathway for developing environmentally friendly materials for advanced water purification applications.

DATA AVAILABILITY

The data supporting the findings of this study are available from the corresponding author upon reasonable request.

DECLARATION OF COMPETING INTEREST

The authors declare that they have no known competing financial interests or personal relationships that could have appeared to influence the work reported in this paper.

FUNDING

The authors declare that no funding was received during the preparation of this manuscript.

References

[1] S. H. Qasim & D. R. Ibrahim, "An overview of azo dyes environmental impacts", GSC Advanced Research and Reviews **24** (2025) 102. https://doi.org/10.30574/gscarr.2025.24.1.0196.

[2] A. P. Periyasamy, "A review of bioremediation of textile dye containing wastewater", Cleaner Water **4** (2025) 100092. https://doi.org/10.1016/j.clwat.2025.100092.

[3] M. Berradi, R. Hsissou, M. Khudhair, M. Assouag, O. Cherkaoui, A. El Bachiri & A. El Harfi, "Textile finishing dyes and their impact on aquatic environs", Heliyon **5** (2019) e02711. https://doi.org/10.1016/j.heliyon.2019.e02711.

[4] S. Khan & D. Borah, "Microbial cell factories in the degradation of azo-dye and their limiting factors: An insight", Cleaner Water **2** (2024) 100034. https://doi.org/10.1016/j.clwat.2024.100034.

[5] R. Al-Tohamy, S. S. Ali, F. Li, K. M. Okasha, Y. A.-G. Mahmoud, T. Elsamahy, H. Jiao, Y. Fu & J. Sun, "A critical review on the treatment of dye-containing wastewater: Ecotoxicological and health concerns of textile dyes and possible remediation approaches for environmental safety", Ecotoxicology and Environmental Safety **231** (2022) 113160. https://doi.org/10.1016/j.ecoenv.2021.113160.

[6] T. E. Oladimeji, M. Oyedemi, M. E. Emetere, O. Agboola, J. B. Adeoye & O. A. Odunlami, "Review on the impact of heavy metals from industrial wastewater effluent and removal technologies", Heliyon **10** (2024) e40370. https://doi.org/10.1016/j.heliyon.2024.e40370.

[7] A. A. Jimoh, B. H. Akpeji, S. I. Aduwa, D. T. Ogundele, M. J. Johnson, S. O. Azeez, P. O. Akusu & M. E. Udezi, ''Microbial assisted biogenic synthesis of titanium dioxide nanoparticles for enhanced methylene blue removal from aqueous solutions'', Discover Chemistry **3** (2026) 92. https://doi.org/10.1007/s44371-026-00541-8.

[8] J. S. Sravan, L. Matsakas & O. Sarkar, ''Advances in biological wastewater treatment processes: Focus on low-carbon energy and resource recovery in biorefinery context'', Bioengineering **11** (2024) 281. https://doi.org/10.3390/bioengineering11030281.

[9] B. Mohan, C. R. Girish, V. R. Murty, G. Jeppu & S. V. Manjunath, ''Advances in the preparation of activated carbon derived from agricultural waste as a sustainable solution for wastewater treatment: A comprehensive review'', Journal of Hazardous Materials Advances **22** (2026) 101128. https://doi.org/10.1016/j.hazadv.2026.101128.

[10] S. Kainth, P. Sharma & O. P. Pandey, ''Green sorbents from agricultural wastes: A review of sustainable adsorption materials'', Applied Surface Science Advances **19** (2024) 100562. https://doi.org/10.1016/j.apsadv.2023.100562.

[11] Z. U. Zango, A. Garba, F. B. Shittu, S. S. Imam, A. Haruna, M. U. Zango, I. A. Wadi, U. Bello, H. Adamu, B. E. Keshta, D. O. Bokov, O. Baigenzhenov & A. Hosseini-Bandegharaei, ''A state-of-the-art review on green synthesis and modifications of ZnO nanoparticles for organic pollutants decomposition and CO2 conversion'', Journal of Hazardous Materials Advances **17** (2025) 100588. https://doi.org/10.1016/j.hazadv.2024.100588.

[12] W. A. Albuquerque, A. J. N. Filho, Y. Romaguera-Barcelay, S. Medina-Carrasco, M. M. Orta, P. Trigueiro & R. R. Peña-Garcia, ''Synergistic ZnO–CuO/halloysite nanocomposite for photocatalytic degradation of ciprofloxacin with high stability and reusability'', Minerals **15** (2025) 977. https://doi.org/10.3390/min15090977.

[13] S. Kanwal, P. Devi, Z. Ahmed & N. A. Qambrani, ''Adsorption isotherm, kinetic and thermodynamic studies for adsorption of fluoride on waste marble powder'', Desalination and Water Treatment **319** (2024) 100441. https://doi.org/10.1016/j.dwt.2024.100441.

[14] O. P. Murphy, M. Vashishtha, P. Palanisamy & K. V. Kumar, ''A review on the adsorption isotherms and design calculations for the optimization of adsorbent mass and contact time'', ACS Omega **8** (2023) 17407. https://doi.org/10.1021/acsomega.2c08155.

[15] M. M. Rahman, M. E. Kabir, M. M. Islam, M. A. B. H. Susan & M. S. Miran, ''Preparation and characterization of porous carbon material from banana pseudo-stem'', Dhaka University Journal of Science **72** (2024) 63. https://doi.org/10.3329/dujs.v72i1.71190.

[16] S. N. Aziz, A. M. Abdulwahab, T. S. Aldeen & A. A. A. Ahmed, ''Tailoring CdO–CuO–ZnO mixed metal oxide nanocomposites for anticancer activity via co-precipitation method'', Nanotechnology, Science and Applications **18** (2025) 225. https://doi.org/10.2147/NSA.S519229.

[17] I. M. Khaled, M. Umair, C. M. Pecoraro, A. Kheniche, M. Bellardita & S. Soltani, ''Green synthesis of ZnO and CuO nanoparticles and ZnO–CuO nanocomposites: Characterization and photocatalytic dyes removal efficiency's determination'', Colloids and Surfaces A: Physicochemical and Engineering Aspects **728** (2026) 138544. https://doi.org/10.1016/j.colsurfa.2025.138544.

[18] S. N. Chandranna, V. N. Hegde, N. C. Sandhya, B. C. Hemaraju & T. M. Pradeep, ''Green synthesised ZnO/CuO nanocomposites for energy storage, environmental remediation and optoelectronic applications'', ChemPhysMater **5** (2026) 107. https://doi.org/10.1016/j.chphma.2025.10.002.

[19] A. BaQais, M. W. Alam, M. Farhan, G. Muteeb, N. Allag & S. Mushtaq, ''Probe-sonicated synthesis of CuO–ZnO hybrid nanocomposite for photocatalytic and supercapacitor applications'', Inorganics **11** (2023) 370. https://doi.org/10.3390/inorganics11090370.

[20] M. Jeevarathinam & I. V. Asharani, ''Synthesis of CuO, ZnO nanoparticles, and CuO–ZnO nanocomposite for enhanced photocatalytic degradation of Rhodamine B: A comparative study'', Scientific Reports **14** (2024) 9718. https://doi.org/10.1038/s41598-024-60008-7.

[21] S. Fakhraddinfakhriazar, C. Molina-Fernandez & G. Leonard, ''Stability of adsorbents for direct air capture (DAC): Challenges and perspectives'', Energy & Fuels **40** (2026) 4930. https://doi.org/10.1021/acs.energyfuels.5c05460.

[22] S. O. Azeez, A. A. Jimoh, I. O. Saheed, K. O. Otun, A. O. Mustapha & F. A. Adekola, ''Optimization by Box–Behnken design for Eosin Yellow dye removal from aqueous medium using date palm seeds-porous carbon@TiO2 blend'', Journal of the Nigerian Society of Physical Sciences **4** (2022) 183. https://doi.org/10.46481/jnsps.2022.533.

[23] B. Vojnovic, M. Cetina, P. Franjkovic & A. Sutlovic, ''Influence of initial pH value on the adsorption of Reactive Black 5 dye on powdered activated carbon: Kinetics, mechanisms, and thermodynamics'', Molecules **27** (2022) 1349. https://doi.org/10.3390/molecules27041349.

[24] D. O. Ozcan, M. C. Hendekci & B. Ovez, ''Enhancing the adsorption capacity of organic and inorganic pollutants onto impregnated olive stone derived activated carbon'', Heliyon **10** (2024) e32792. https://doi.org/10.1016/j.heliyon.2024.e32792.

[25] M. Salman, M. Demir, K. H. D. Tang, L. T. T. Cao, S. Bunrith, T.-W. Chen, N. M. Darwish, B. M. AlMunqedhi & T. Hadibarata, ''Removal of Cresol Red by adsorption using wastepaper'', Industrial and Domestic Waste Management **2** (2022) 1. https://doi.org/10.53623/idwm.v2i1.63.

[26] M. Akhtar, M. Sarfraz, M. Ahmad, N. Raza & L. Zhang, ''Use of low-cost adsorbent for waste water treatment: Recent progress, new trend and future perspectives'', Desalination and Water Treatment **321** (2025) 100914. https://doi.org/10.1016/j.dwt.2024.100914.

[27] G. B. Adebayo, F. A. Adekola, A. A. Jimoh, F. O. Alao & H. I. Adegoke, ''Adsorption of Cd(II) ions from aqueous solution using activated carbon prepared from Vitellaria paradoxa shell'', NSTI Advanced Materials TechConnect Briefs **3** (2015) 249. https://briefs.techconnect.org/papers/adsorption-of-cd-ii-ions-from-aqueous-solution-using-activated-carbon-prepared-from-vitellaria-paradoxa-shell/.

[28] P. Amaechi, C. Elenwo & S. O. N. Dimkpa, ''Langmuir and Freundlich isotherm models' description of P adsorption capacity of wetland and upland soil in Rivers State'', Global Journal of Agricultural Research **12** (2024) 14. https://doi.org/10.37745/gjar.2013/vol12n31429.

[29] S. Kalam, S. A. Abu-Khamsin, M. S. Kamal & S. Patil, ''Surfactant adsorption isotherms: A review'', ACS Omega **6** (2021) 32342. https://doi.org/10.1021/acsomega.1c04661.

[30] Y. T. Huang & M. C. Shih, ''Kinetic, isotherm, and thermodynamic modeling of Methylene Blue adsorption using natural rice husk: A sustainable approach'', Separations **12** (2025) 189. https://doi.org/10.3390/separations12080189.

[31] N. Idrissov, N. Aidarbekov, Z. Kuspanov, K. Askaruly, O. Tsurtsumia, K. Kuterbekov, Z. Zeinulla, K. Bekmyrza, A. Kabyshev, M. Kubenova & A. Serik, ''Effect of metal modification of activated carbon on the hydrogen adsorption capacity'', Nanomaterials **15** (2025) 1503. https://doi.org/10.3390/nano15191503.

[32] J. Lach & E. Okoniewska, ''Equilibrium, kinetic, and diffusion mechanism of lead(II) and cadmium(II) adsorption onto commercial activated carbons'', Molecules **29** (2024) 2418. https://doi.org/10.3390/molecules29112418.